ACS SENSORS

pubs.acs.org/acssensors

Article

Triplet-Triplet Annihilation Upconversion Based Nanosensors for Fluorescence Detection of Potassium

Megan P. Jewell, Meredith D. Greer, Alexandra L. Dailey, and Kevin J. Cash*

Cite This: *ACS Sens.* 2020, 5, 474−480

Read Online

ACCESS | Metrics & More | Article Recommendations | Supporting Information

ABSTRACT: Typical ionophore-based nanosensors use Nile blue derived indicators called chromoionophores, which must contend with strong background absorption, autofluorescence, and scattering in biological samples that limit their usefulness. Here, we demonstrate potassium-selective nanosensors that utilize triplet-triplet annihilation upconversion to minimize potential optical interference in biological media and a pH-sensitive quencher molecule to modulate the upconversion intensity in response to changes in analyte concentration. A triplet-triplet annihilation dye pair (platinum(II) octaethylporphyrin and 9,10-diphenylanthracene) was integrated into nanosensors containing an analyte binding ligand (ionophore), charge-balancing additive, and a pH indicator quencher. The nanosensor response to potassium was shown to be reversible and stable for 3 days. In addition, the nanosensors are selective against sodium, calcium, and magnesium (selectivity coefficients in $\log_{10}$ units of −2.2 for calcium, −2.0 for sodium, and −2.4 for magnesium), three interfering ions found in biological samples. The lack of signal overlap between the upconversion nanosensors and GFP, a common biological fluorescent indicator, is demonstrated in confocal microscope images of sensors embedded in a bacterial biofilm.

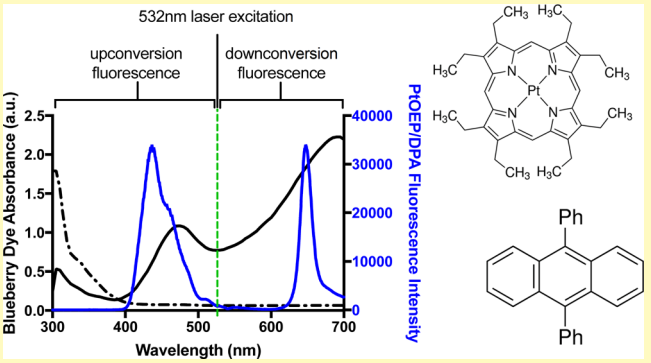

KEYWORDS: *sensor, triplet-triplet annihilation, upconversion, biosensor, ionophore-based optical sensor*

Selective and tunable ion detection and imaging in biological and environmental samples are essential in a range of investigations. Sensors that are capable of continuous and long-term monitoring of biological processes, both in vitro and in vivo, allow for interrogation to answer basic research questions and monitor health in a clinical setting. The many potential analytes of interest and the development of sensors for them have been extensively reviewed and summarized elsewhere.[1−6] In particular, Ruckh and Clark discussed the importance of continuous physiological monitoring of analytes such as sodium, potassium, and glucose for conditions such as renal failure and diabetes.[1] Sensors for detection of other electrolytes like calcium and lithium are discussed in reviews by Søndergaard et al.[3] and Rong et al.[2]

Ionophore-based optical sensors (IBOSs) are a class of indirect ion-selective optical sensors that have been used to measure a wide range of analytes in vitro,[7,8] in situ,[9] and in vivo.[10,11] These sensors utilize a mechanism similar to ion-selective electrodes and are well described elsewhere.[12,13] Typically, IBOSs are composed of a pH indicator, an analyte-binding ligand (ionophore), and a charge-balancing additive suspended in a highly plasticized hydrophobic polymer matrix, which is surrounded by a lipid layer. As the target ion binds to the ionophore, the pH indicator is deprotonated in order to maintain electroneutrality within the polymer matrix. Based on the well-established ion exchange theory,[13] this change in protonation can be monitored via absorbance or fluorescence measurements. Because the recognition element (ionophore) is decoupled from the signaling element (pH indicator), nanosensors for different ions are easily created without the need to design new recognition mechanisms.[14] Thus, the potassium-selective nanosensors described here can easily be made selective for another ion by exchanging the ionophore, and other components are also able to be substituted.[15]

The signaling elements utilized by most IBOSs are Nile blue derivative pH indicators (chromoionophores).[14] Some methods that avoid pH cross-reactivity are also utilized.[16,17] Recent work in ionophore-based nanosensors has included the use of silicon-based particles[18] as well as carbon dots (aka graphene quantum dots)[19−21] as signaling elements as well. However, these dyes, and indeed most fluorescent dyes, must contend with strong background absorption, autofluorescence, and scattering in biological samples, which can significantly limit their application.[22] Our solution to some of these issues is to use materials with the unique property of upconversion. These

Received: November 14, 2019
Accepted: January 8, 2020
Published: January 8, 2020

https://dx.doi.org/10.1021/acssensors.9b02252
ACS Sens. 2020, 5, 474−480

materials exhibit an anti-Stokes shift under excitation that allows their signal to be easily distinguished from the autofluorescence and background interference of biological tissues and samples.[4] Lanthanide-based upconversion, which has been used extensively as a biological imaging component[23−25] and is well described,[26,27] utilizes lanthanide ions doped into a crystalline lattice as emissive centers. There are several reports of lanthanide-based bulk optodes capable of sensing pH, Pb^{2+}, K^+, Na^+, Ca^{2+}, and Cu^{2+}.[28,29] However, there are several drawbacks to lanthanide-based upconversion materials. The primary drawback is the relatively low upconversion efficiency, which then requires relatively high-power-density excitation for any substantive imaging.[26] Another drawback for use on the nanoscale is the size of lanthanide-based materials. Because these materials are sensitive to surface deactivations, the high surface-to-volume ratio of nanoparticles can decrease upconversion efficiency.[30] Although core/shell structures can mitigate this problem, many lanthanide particles used in sensing are on the order of hundreds of nanometers in size,[28,29,31,32] which precludes their use in polymeric nanoparticle systems like our IBOS, which are only 100 nm in diameter.[33,34]

An alternate upconversion mechanism, which we utilize in this work, is triplet-triplet annihilation upconversion (TTA-UC). As opposed to the inorganic lanthanide-based system, TTA-UC utilizes organic molecules known as sensitizers and emitters to produce upconversion luminescence. In this process, the sensitizer absorbs excitation light and populates its first singlet excited state. After intersystem crossing to the triplet state, there is triplet-triplet energy transfer between the sensitizer and emitter.[35] Triplet-triplet annihilation occurs between two excited emitter molecules, and this energy populates the first singlet excited state of one of the emitter molecules, which then produces delayed fluorescence.[35] Common examples of sensitizer dyes are metal-centered porphyrins, and commonly used emitters are high luminescence quantum yield dyes such as 9,10-diphenylanthracene or BODIPY.[26] In comparison to lanthanide systems, TTA-UC requires relatively low power excitation[26] and can be wavelength-tuned by the choice of sensitizer and annihilator. The sensitizer-annihilator dye pairs are organic dyes that are often commercially available, soluble in the organic phase, and able to be implemented into IBOS. TTA-UC has been utilized in several forms as a biological imaging agent.[26] There are in vivo[36−41] and in vitro[25,42−44] examples that have overcome the problem of oxygen quenching of TTA-UC. However, TTA-UC has found limited application in sensing platforms. Thus far, it has been limited to Borisov et al.[45] creating a polymer optode film to directly sense oxygen. However, there are already numerous optical oxygen sensing platforms available.[5,6] To our knowledge, there have been no reports of TTA-UC used in a more general sensing platform such as those based on ionophores. TTA-UC is not inherently sensitive to ion concentration, so in this work, it is coupled with a pH-sensitive quencher dye that modulates the signal that has been utilized previously to gate other optically static systems.[33,46,47]

MATERIALS AND METHODS

Materials. Poly(vinyl chloride) (high molecular weight, (PVC)), tetrahydrofuran (THF), dichloromethane (DCM), sodium tetrakis-[3,5-bis(trifluoromethyl)phenyl]borate (NaBARF; Selectophore), 2-dodecyl-2-methyl-1,3-propanediyl bis[*N*-[5′-nitro(benzo-15-crown-5)-4′-yl]carbamate] (potassium ionophore III, Selectophore), platinum(II) octaethylporphyrin (PtOEP), bis(2-ethylhexyl) sebacate (DOS/BEHS, Selectophore), and soybean oil were purchased from Sigma-Aldrich (St. Louis, MO, USA). 9,10-Diphenylanthracene (DPA) was purchased from Acros Organics. 1,2-Dipalmitoyl-*sn*-glycero-3-phosphoethanolamine-*N*-[methoxy(polyethylene glycol)-750] ammonium salt in chloroform (PEG-lipid) was purchased from Avanti Polar Lipids (Alabaster, AL). 2-[4-(2-Hydroxyethyl)-piperazin-1-yl]ethanesulfonic acid (HEPES; Molecular Biology grade), 2-amino-2-hydroxymethylpropane-1,3-diol (Tris; 2 M), potassium chloride (KCl), hydrochloric acid concentrate (HCl; 10 N, ACS certified), and sodium hydroxide concentrate (NaOH; 10 N, ACS certified) were purchased from Fisher Scientific (Waltham, MA, USA). Blueberry-C6-ester-652 was purchased from Berry & Associates, Inc. (Dexter, MI, USA).

Nanosensor Fabrication. 57.4 mg of poly(vinyl chloride) (PVC) was weighed into a 2 mL vial, and 38.4 μL of soybean oil was added. This vial was then vortexed for 1 min. In a separate vial, 2.9 mg of 9,10- diphenylanthracene (DPA), 0.185 mg of platinum octaethylporphyrin (PtOEP), 1 mg of potassium ionophore III (KI3), 1 mg of blueberry-C6-ester-652 (blueberry), and 1 mg of NaBARF were dissolved in 585 μL of tetrahydrofuran (THF). THF and dissolved dyes were then added to the PVC/soybean oil mixture and vortexed thoroughly for 1 min. This mixture of components (PVC, soybean oil, and dyes suspended in solvent)—called the optode cocktail (a precursor for optode formation)—was then stored at 4 °C.

Nanosensors were prepared in a manner similar to that described by Billingsley et al.[48] The optode cocktail was spread on a glass surface and allowed to dry for at least 30 min. The dried optode film was then transferred to a 4 dram scintillation vial that was charged with 3 mL of HEPES/Tris solution (10 mM HEPES/6 mM Tris buffer at pH = 7.4) along with 5 mg (25 mg/mL in 200 μL of chloroform) of 1,2-dipalmitoyl-*sn*-glycero-3-phosphoethanolamine-*N*-[methoxy(polyethylene glycol)-750] ammonium salt in chloroform (PEG-lipid). The vial was agitated by hand to ensure that the optode was suspended in the PEG-lipid/chloroform phase. The solution was then emulsified with a probe-tip sonicator (Branson) at 40% amplitude for 3 min. The emulsion was then filtered with a 0.8 μm Supor Membrane filter (Pall Corporation) to remove excess components.

Nanosensor Characterization. The nanosensors' fluorescence response was calibrated with KCl test solutions prepared at double the desired final concentration in HEPES/Tris buffer solution (pH = 7.4). 300 μL of nanosensor solution and 300 μL of KCl test solution were mixed in screw-top quartz cuvettes (Starna cells, Atascadero, CA) to achieve the desired final analyte concentration. Response curves were generated by collecting fluorescence intensities with an excitation of 532 nm and an emission of 435 nm. Values were normalized between the endpoint responses. A four-parameter logistic response curve was applied with GraphPad Prism 7 software (GraphPad, La Jolla, CA, USA) to determine response characteristics.

Fluorescence measurements were performed on an Avantes StarLine spectrometer (Avantes, Louisville, CO), and absorbance measurements were performed on a Synergy H1 microplate reader using Nunc MicroWell 96-Well Optical-Bottom Plates with Polymer Base (Nalgene Nunc International, Roskilde, Denmark). All fluorescence measurements were performed with 532 nm laser excitation from a 5 mW laser (Z-Bolt, Clackamas, OR) through a 600 μm fiber (Avantes) unless otherwise stated. Dynamic light scattering, zeta potential, and mobility measurements were performed on a Brookhaven ZetaPALS with Particle Solutions software V 2.2 (Brookhaven Instruments Corporation, Holtsville, NY). For reversibility measurements, nanosensors were concentrated ∼10× via ultrafiltration (Amicon Ultracel) and immobilized in microdialysis tubing (MWCO 13 kDa, Spectrum Laboratories) on the bottom of a 4-well Lab-Tek Chamber Slide using underwater epoxy.[49] The chamber slide was placed on the microscope stage, and solutions of either 10^{-8} M or 2 M KCl in HEPES/Tris (pH = 7.4) were exchanged three times each, with washes of HEPES/Tris between each exchange. Nanosensors were excited at 514 nm, and emission from 400 to 450 nm was recorded as a single image using a Zeiss

https://dx.doi.org/10.1021/acssensors.9b02252
ACS Sens. 2020, 5, 474−480

LSM780 confocal microscope (Zeiss, Switzerland). Images were analyzed using ImageJ.

Upconversion nanosensor (UCNS) shelf stability was monitored over 4 days. 24 batches of UCNS were synthesized as described above and combined to obtain the necessary volume. The nanosensors were stored in the dark at room temperature. On days 1, 2, 3, and 4, triplicate 300 μL aliquots were combined with 300 μL of KCl in HEPES/Tris (pH = 7.4) solution to produce a response curve. Nanosensor photostability was performed using the Avantes StarLine spectrometer and Starna screw-top cuvettes. Fresh UCNS were prepared as described, and 600 μL was injected into the cuvettes. Emission at 435 nm with continuous excitation at 532 nm was monitored every 20 s for 60 min. To test temperature and oxygen sensitivity of UCNS, 300 μL of nanosensors was mixed with 300 μL of KCl test solutions in screw-top quartz cuvettes. Measurements were made at room temperature and ambient oxygen concentration. Then the mixtures were either incubated at 37 °C for 20 min or deoxygenated with N_2 for 20 min, and measurements were made again.

Embedded Nanosensor Imaging. UCNSs were prepared as described above and concentrated ~10× via ultrafiltration (Amicon Ultracel). Traditional downconversion nanosensors (KNSs) were prepared as described by Dubach et al.,[50] swapping potassium ionophore III for sodium ionophore X. The nanosensors were then concentrated ~10× via ultrafiltration. Biofilm growth procedures were adapted from methods by Kirchner et al.[51] and Jewell et al.[52] Briefly, *Pseudomonas aeruginosa* strain PAO1 (ATCC 15692) was plated onto Luria Bertani (LB) agar (Sigma-Aldrich, St. Louis, MO, USA) from frozen stocks and incubated at 37 °C for 24 h. One colony was dispersed in 1 mL of LB broth and incubated for 24 h at 37 °C. Liquid culture was diluted to an optical density (OD_{600}) of 0.05. Biofilms were grown statically in a 16.7% v/v solution of either UCNS or KNS in 10 mM HEPES/6 mM Tris buffer mixed with LB broth (Sigma-Aldrich). A total of 600 μL of nanosensors + LB was added to each well of a 4-well Lab-Tek Chamber Slide and then inoculated with an inoculation loopful of liquid *P. aeruginosa* culture at an OD_{600} of 0.05. The chamber slides were placed in a humidity chamber and incubated for 24 h at 37 °C.

RESULTS AND DISCUSSION

We chose the TTA-UC pair of PtOEP and DPA based on previous work by Islangulov et al.[53] and others[54−56] on embedding TTA-UC sensitizers and emitters in polymer films, polymer nanoparticles, and microemulsions. Our first step was optimizing the formulation of the TTA-UC system in our sensor matrix materials. Figure S1 shows that using a platinum centered porphyrin (PtOEP) combined with DPA produced stronger upconversion luminescence than a similar palladium-based system (PdOEP/DPA) in the chosen PVC/soybean oil matrix when added at the same concentrations. The soybean oil acted as both the plasticizer (replacing the more traditional DOS) and a protectant against oxygen quenching (Figure S2).[36] However, the soybean oil's ability to scavenge oxygen radicals was not indefinite, which was seen in a loss of response by day 3 after synthesis (Figure S3).

Both PtOEP and DPA were incorporated into the ionophore-based nanosensor platform. Figure 1 illustrates the overlap of the TTA-UC emission spectrum and the absorbance spectra of the protonated and non-protonated states of the blueberry dye.

The mechanism of ion exchange for a system that contains blueberry as the pH indicator is described in detail elsewhere.[33] The sensor mechanism is shown in Figure 2, where at low K^+ concentrations, the blueberry dye is protonated (low absorbance) and the upconversion signal is not quenched. At higher K^+ concentrations, K^+ ions bind to the ionophore and

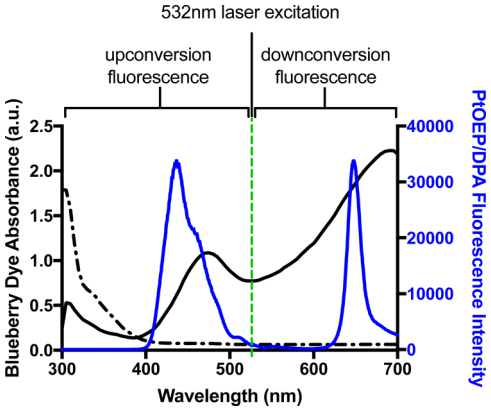

Figure 1. Blueberry dye absorbance spectra (black) in either protonated (black, dash-dot) or deprotonated (black, solid) state. The TTA-UC spectrum of PtOEP/DPA (blue) at 532 nm excitation shows an excellent overlap between blueberry dye absorbance peaks at 690 and 480 nm.

protons from the blueberry dye are displaced to maintain electroneutrality. The deprotonated blueberry has an absorbance peak at 480 nm that overlaps with the PtOEP emission at 435 nm, gating the upconversion fluorescence. Previous work by Sahari et al.[46] determined that the apparent pK_a of blueberry is 7.85, which is within the relevant range for biological applications.

Emission spectra of TTA-UC nanosensor fluorescence responses to K^+ concentrations in oxygenated conditions at 532 nm excitation (Figure 3) were calibrated from 10^{-8} to 1 M K^+. The sensors have a response midpoint of 60 μM K^+ and a linear range of 8 to 260 μM. When deoxygenated, the UCNS has a response midpoint of 0.82 mM K^+. In deoxygenated conditions, the sensors have a linear range of 0.09 to 3.8 mM. The normalized response can be seen in Figure S4. This difference in response may be due to differences in overall brightness or batch-to-batch variability.

Solutions of sodium, calcium, and magnesium chloride salts (0−0.1 M) in HEPES/Tris were also tested (Figure 4) to evaluate UCNS selectivity and resulted in response midpoints of 9.3 mM $CaCl_2$ and 7 mM for NaCl. Comparison of Ca^{2+} with the response midpoint for K^+ resulted in a selectivity coefficient (in $\log_{10}$ units) of −2.2. When compared with the response midpoint for Na^+, the selectivity coefficient is −2.0. This is slightly larger than was found in optodes synthesized using potassium ionophore III by Shortreed et al.[57] Sahari et al.[46] noted increased selectivity for K^+ over Na^+ in K^+-selective nanosensors containing blueberry dye that utilized traditional downconversion fluorescence. This indicates that there may be an interaction between K^+ ions and blueberry. Compared with prior work,[18] the selectivity against calcium and magnesium for these sensors is slightly diminished, potentially as a result of the upconversion signaling groups. These sensors are thus selective against potentially interfering ions most commonly found in biological systems. This does not include potential interference from H^+ ions as the mechanism demonstrated here is inherently pH-dependent. However, as demonstrated in Figures 3 and 4, in a well-buffered in vitro environment, these sensors respond primarily to K^+. These sensors could be made pH-insensitive through the use of solvatochromic dyes as others have shown.[20,21,58,59]

Figure S11 shows a small temperature sensitivity at lower concentrations (increased intensities) that can be accounted

https://dx.doi.org/10.1021/acssensors.9b02252
ACS Sens. 2020, 5, 474−480

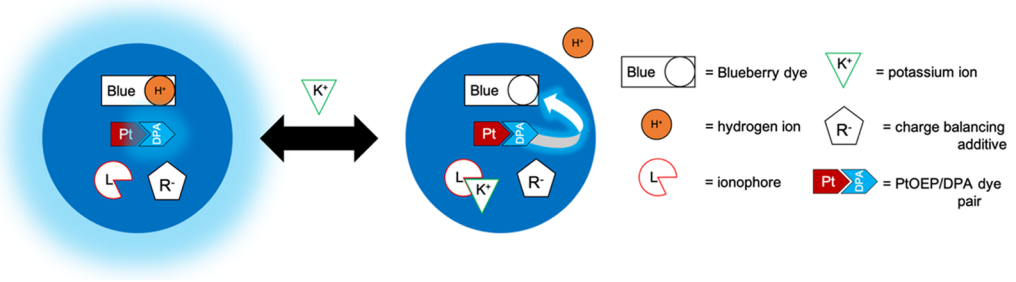

Figure 2. Schematic of nanosensor components coloaded into the nanosensor matrix and fluorescence gating mechanism in response to decreasing potassium (K^+) concentrations.

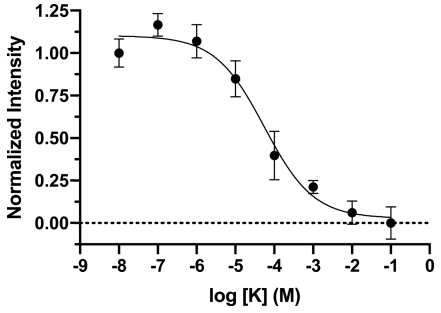

Figure 3. Normalized fluorescence intensity of UCNS response to KCl solution buffered in HEPES/Tris (pH = 7.4).

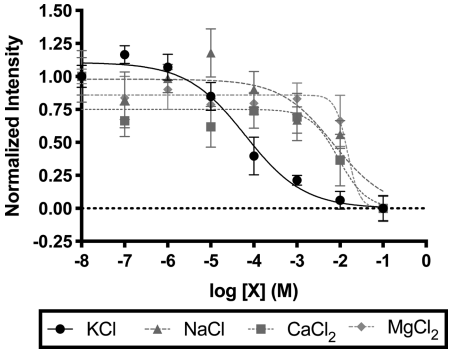

Figure 4. Normalized fluorescence intensity of UCNS response to NaCl, KCl, $MgCl_2$, and $CaCl_2$ solution buffered in HEPES/Tris (pH = 7.4).

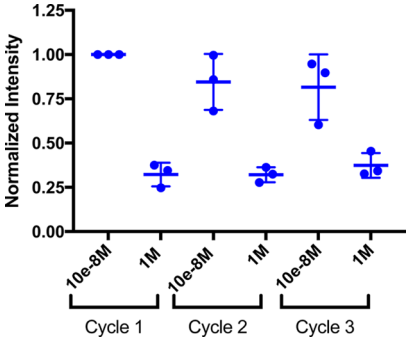

Figure 5. UCNS reversibility in dialysis tubes. The figure shows mean intensities of three trials of tubes for three washes of 0 M KCl and three washes of 1 M KCl demonstrating reversibility of the sensor mechanism. Error bars represent standard deviation.

for as long as calibration is performed under similar, controlled conditions. Similarly, there is some oxygen sensitivity that remains (Figure S12) even with the use of soybean oil as an oxygen scavenger. This prevents use in systems with a nonuniform oxygen concentration, for example, organoids, where oxygen is significantly diffusion-limited. Potential improvements might include addition of another oxygen scavenger, such as BSA-dextran[36] or hyperbranched polyphosphates.[60]

As expected, the UCNSs are reversible, demonstrated under controlled conditions using UCNS in 13 kD MWCO microdialysis fibers via confocal microscopy. Solutions of 10^{-8} or 1 M KCl in HEPES/Tris (pH = 7.4) were added to the chamber slide wells containing fibers filled with UCNS. The fluorescence intensity at 400−450 nm (514 nm excitation) was measured to produce Figure 5. The 10^{-8} to 1 M KCl cycles were repeated three times, with washes of HEPES/Tris buffer (pH = 7.4) in between each solution change. The signal intensity returns when the sensors are exposed to 10^{-8} M KCl after 1 M KCl exposure, so the UCNSs are reversible, as expected based on the equilibrium-based sensing mechanism.[61] There is some loss of signal over the three cycles measured, which may be due to photobleaching (see Figure S5).

We also determined the batch-to-batch variability between four sensor batches whose response curves are shown in Figure S7. One-way ANOVA reveals no significant difference between the log values of the response midpoint of each batch or the sensitivity values (slope) of the response curve. This indicates that batches can be fabricated reproducibly as long as they are produced from the same initial optode. One point to note is that Galyean et al.[33] noted that there was variance in blueberry response between lots, which may account for variance between optodes that were synthesized with the blueberry dye.

The shelf stability of the UCNS was determined based on the potassium response curve as well as the nanosensor hydrodynamic diameter and zeta potential. All of these were monitored over 4 days and are shown in Figure S3 and Table 1. The change in response midpoint observed coincides with a decrease in overall fluorescence intensity. By day 4, there is only a slight response to solutions of 0.1 and 1 M KCl. It is believed that this is due to oxidative destruction of sensor components as the soybean oil loses its oxygen scavenging ability, or additive leakage, as the decrease in fluorescence intensity stabilizes by day 3 but the change in response does not.

The only notable change in physical properties beyond the sensor response is an increase in hydrodynamic diameter by day 4. The increase from approximately 105 to 124 nm is small but is statistically significant ($p < 0.05$). This may indicate that the nanoparticles are beginning to aggregate.

https://dx.doi.org/10.1021/acssensors.9b02252
ACS Sens. 2020, 5, 474−480

Table 1. Characterization of Nanosensors on days 1, 2, and 4 with Dynamic Light Scattering and Phase Analysis Light Scattering

day	eff. diameter (nm)	polydispersity	zeta potential (mV)	mobility (μm s^{-1} (V cm^{-1})$^{-1}$)	log(EC_{50}) (M)
day 1	105.6 ± 2.4	0.34 ± 0.01	−40.9 ± 1.8	−3.2 ± 0.1	−3.08 ± 0.15
day 2	104.0 ± 5.9	0.33 ± 0.00_4	−46.2 ± 2.7	−3.6 ± 0.2	−3.01 ± 0.29
day 4	123.8 ± 5.3	0.34 ± 0.00_4	−42.9 ± 3.4	−3.4 ± 0.3	−0.987 ± 0.15

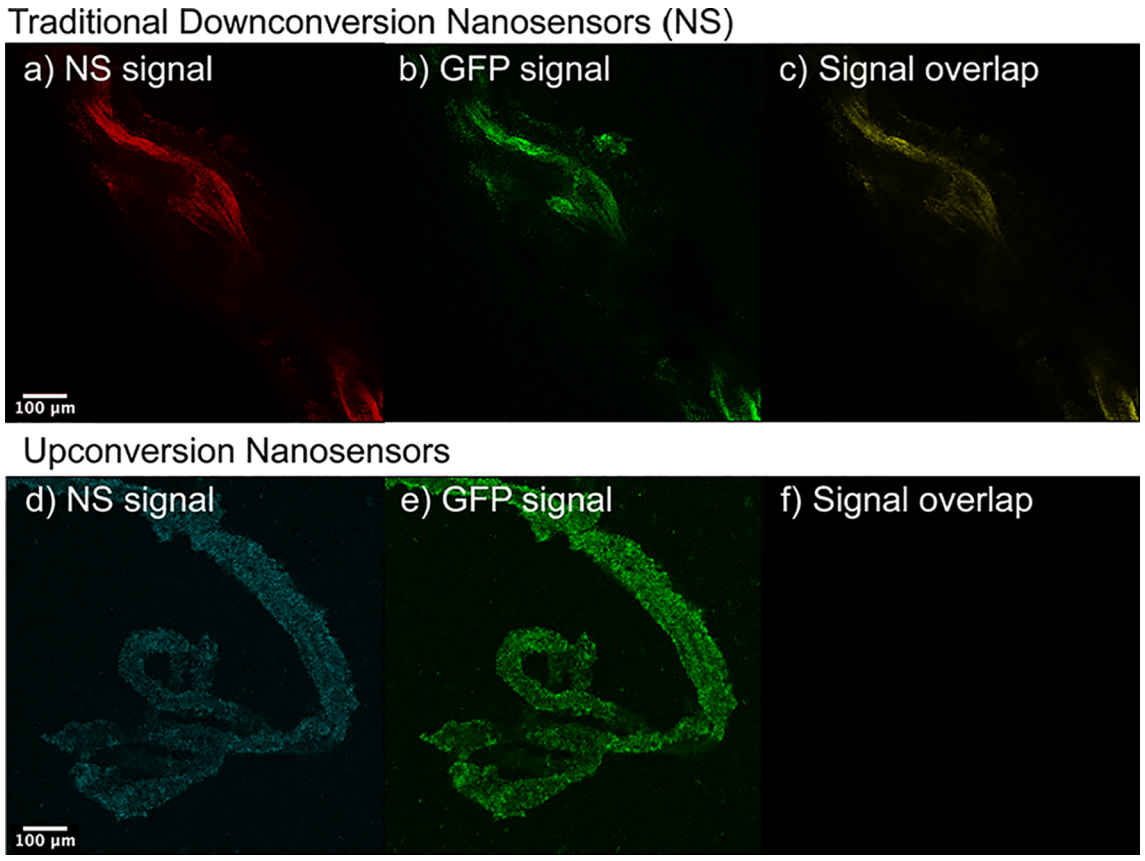

Figure 6. (top) Traditional downconversion nanosensors utilizing rhodamine B as one of the elements, embedded in a *P. aeruginosa* biofilm. (a) Signal from the rhodamine B reporter, excited at 514 nm and emission recorded over 535−632 nm. (b) Signal from GFP-expressing *P. aeruginosa* PAO1, excited at 488 nm and emission recorded over 500−560 nm. (c) Signal overlap between GFP and rhodamine B, excited at 488 nm and emission recorded over 540−590 nm. (bottom) Upconversion nanosensors described in this manuscript embedded in a *P. aeruginosa* biofilm. (d) Signal from PtOEP/DPA dye pair, excited at 514 nm and emission recorded over 400−500 nm. (e) Signal from GFP-expressing *P. aeruginosa* PAO1 excited at 488 nm and emission recorded over 500−600 nm. (f) Signal overlap between GFP and PtOEP/DPA dye pair, excited at 514 nm and emission recorded over 490−514 nm. This demonstrates that the upconversion signal successfully reduces the optical overlap.

The UCNS were compared with traditional downconversion nanosensors (KNSs) in an in vitro biological system. Biofilms of *P. aeruginosa* strain PAO1 that expresses GFP were grown and incorporated either UCNS or KNS into their extracellular polymeric substance. The biofilms were imaged with confocal microscopy, and these images can be seen Figure 6. The emission spectra of the KNS, which overlaps with the GFP emission spectra, produce a significant amount of signal overlap that makes quantification of the KNS signal difficult. When the KNSs are replaced with UCNS, the GFP and nanosensor signals can be imaged with a minimal overlap.

CONCLUSIONS

Here, we have demonstrated a nanosensor platform to quantify potassium concentrations that incorporates triplet-triplet annihilation upconversion and a pH-sensitive quencher dye. These TTA-UC nanosensors are capable of sensing physiologically relevant K^+ concentrations, selective against Na^+, Ca^{2+}, and Mg^{2+}, reversible, and demonstrate a stable response for 3 days. Further work is needed to identify a reference dye that does not interact with the blueberry dye or the TTA-UC process to allow for a ratiometric response. Because of the blueberry dye's wide absorbance spectrum, an NIR or IR dye might make ratiometric measurements possible with low tissue interference. Alternatively, the pH-dependent blueberry dye might be replaced with a solvatochromic dye.[59] This would also eliminate any interference from pH changes within the system. This type of future work would allow for correction for environmental and nanosensor concentration changes and future in vitro and in vivo studies.

ASSOCIATED CONTENT

Supporting Information

The Supporting Information is available free of charge at https://pubs.acs.org/doi/10.1021/acssensors.9b02252.

https://dx.doi.org/10.1021/acssensors.9b02252
ACS Sens. 2020, 5, 474−480

(Figure S1) Emission spectra of TTA-UC dye pairs in PVC/DOS films, (Figure S2) spectra of upconversion luminescence in nanoparticles containing soybean oil vs DOS, (Figure S3) upconversion nanosensor response to KCl in an oxygenated environment, (Figure S4) lifetime response of UCNS, (Figure S5) photostability of upconversion nanosensors, (Figure S6) photostability plot with error bars shown, (Figure S7) batch-to-batch variability of UCNS produced from the same initial optode, (Figure S8) representative confocal microscopy images of UCNS in microdialysis fibers, (Figure S9) raw (non-normalized) intensity data for UCNS lifetime measurements, (Figure S10) raw (non-normalized) intensity data for UCNS selectivity against different ions, (Figure S11) temperature sensitivity data of UCNS at high- and low-K^+ concentrations, and (Figure S12) oxygen sensitivity data of UCNS at high- and low-K^+ concentrations (PDF)

AUTHOR INFORMATION

Corresponding Author

Kevin J. Cash − *Colorado School of Mines, Golden, Colorado;* orcid.org/0000-0002-9748-2530; Email: kcash@mines.edu

Other Authors

Megan P. Jewell − *Colorado School of Mines, Golden, Colorado*

Meredith D. Greer − *Colorado School of Mines, Golden, Colorado*

Alexandra L. Dailey − *Colorado School of Mines, Golden, Colorado*

Complete contact information is available at: https://pubs.acs.org/10.1021/acssensors.9b02252

Notes

The authors declare no competing financial interest.

ACKNOWLEDGMENTS

This work was supported by start-up funds from Colorado School of Mines. Imaging experiments were performed in the University of Colorado Anschutz Medical Campus Advance Light Microscopy Core supported in part by NIH/NCATS Colorado CTSI Grant Number UL1 TR001082. Contents are the authors' sole responsibility and do not necessarily represent official NIH views.

ABBREVIATIONS

TTA-UC, triplet-triplet annihilation upconversion; UCNS, upconversion nanosensor; KNS, potassium-selective nanosensor

REFERENCES

(1) Ruckh, T. T.; Clark, H. A. Implantable nanosensors: Toward continuous physiologic monitoring. *Anal. Chem.* **2014**, *86*, 1314−1323.

(2) Rong, G.; Corrie, S. R.; Clark, H. A. In Vivo Biosensing: Progress and Perspectives. *ACS Sens.* **2017**, *2*, 327−338.

(3) Søndergaard, R. V.; Christensen, N. M.; Henriksen, J. R.; Kumar, E. K. P.; Almdal, K.; Andresen, T. L. Facing the Design Challenges of Particle-Based Nanosensors for Metabolite Quantification in Living Cells. *Chem. Rev.* **2015**, *115*, 8344−8378.

(4) Wang, C.; Li, X.; Zhang, F. Bioapplications and biotechnologies of upconversion nanoparticle-based nanosensors. *Analyst* **2016**, *141*, 3601−3620.

(5) Roussakis, E.; Li, Z.; Nichols, A. J.; Evans, C. L. Oxygen-Sensing Methods in Biomedicine from the Macroscale to the Microscale. *Angew. Chem., Int. Ed.* **2015**, *54*, 8340−8362.

(6) Wolfbeis, O. S. Luminescent sensing and imaging of oxygen: Fierce competition to the Clark electrode. *BioEssays* **2015**, *37*, 921−928.

(7) Rong, G.; Kim, E. H.; Poskanzer, K. E.; Clark, H. A. A method for estimating intracellular ion concentration using optical nanosensors and ratiometric imaging. *Sci. Rep.* **2017**, *7*, 10819.

(8) Dubach, J. M.; Das, S.; Rosenzweig, A.; Clark, H. A. Visualizing sodium dynamics in isolated cardiomyocytes using fluorescent nanosensors. *Proc. Natl. Acad. Sci.* **2009**, *106*, 16145−16150.

(9) Church, J.; Armas, S. M.; Patel, P. K.; Chumbimuni-Torres, K.; Lee, W. H. Development and Characterization of Needle-type Ion-selective Microsensors for in situ Determination of Foliar Uptake of Zn^{2+} in Citrus Plants. *Electroanalysis* **2018**, *30*, 626−632.

(10) Cash, K. J.; Li, C.; Xia, J.; Wang, L. V.; Clark, H. A. Optical Drug Monitoring: Photoacoustic Imaging of Nanosensors to Monitor Therapeutic Lithium in Vivo. *ACS Nano* **2015**, *9*, 1692−1698.

(11) Balaconis, M. K.; Clark, H. A. Biodegradable optode-based nanosensors for in vivo monitoring. *Anal. Chem.* **2012**, *84*, 5787−5793.

(12) Bakker, E.; Bühlmann, P.; Pretsch, E. Carrier-Based Ion-Selective Electrodes and Bulk Optodes. 1. General Characteristics. *Chem. Rev.* **1997**, *97*, 3083−3132.

(13) Mistlberger, G.; Crespo, G. A.; Bakker, E., Ionophore-Based Optical Sensors. In *Annual Review of Analytical Chemistry, Vol 7*; Cooks, R. G.; Pemberton, J. E., Eds. Annual Reviews: Palo Alto, 2014; Vol. 7, pp 483−512.

(14) Xie, X.; Bakker, E. Ion selective optodes: from the bulk to the nanoscale. *Anal. Bioanal. Chem.* **2015**, *407*, 3899−3910.

(15) Cánovas, R.; Padrell Sánchez, S.; Parrilla, M.; Cuartero, M.; Crespo, G. A. Cytotoxicity Study of Ionophore-Based Membranes: Toward On Body and in Vivo Ion Sensing. *Acs Sens.* **2019**, *4*, 2524−2535.

(16) Xie, X. J.; Zhai, J. Y.; Bakker, E. pH Independent Nano-Optode Sensors Based on Exhaustive Ion-Selective Nanospheres. *Anal. Chem.* **2014**, *86*, 2853−2856.

(17) Xie, X. Renovating the chromoionophores and detection modes in carrier-based ion-selective optical sensors. *Anal. Bioanal. Chem.* **2016**, *408*, 2717−2725.

(18) Du, X.; Yang, L.; Hu, W.; Wang, R.; Zhai, J.; Xie, X. A Plasticizer-Free Miniaturized Optical Ion Sensing Platform with Ionophores and Silicon-Based Particles. *Anal. Chem.* **2018**, *90*, 5818−5824.

(19) Arshad, F.; Pal, A.; Rahman, M. A.; Ali, M.; Khan, J. A.; Sk, M. P. Insights on the solvatochromic effects in N-doped yellow-orange emissive carbon dots. *New J. Chem.* **2018**, *42*, 19837−19843.

(20) Mei, S.; Wei, X.; Hu, Z.; Wei, C.; Su, D.; Yang, D.; Zhang, G.; Zhang, W.; Guo, R. Amphipathic carbon dots with solvent-dependent optical properties and sensing application. *Opt. Mater.* **2019**, *89*, 224−230.

(21) Zheng, M.; Li, Y.; Zhang, Y.; Xie, Z. Solvatochromic fluorescent carbon dots as optic noses for sensing volatile organic compounds. *RSC Adv.* **2016**, *6*, 83501−83504.

(22) Zhou, J.; Liu, Z.; Li, F. Upconversion nanophosphors for small-animal imaging. *Chem. Soc. Rev.* **2012**, *41*, 1323−1349.

(23) Liang, T.; Li, Z.; Song, D.; Shen, L.; Zhuang, Q.; Liu, Z. Modulating the Luminescence of Upconversion Nanoparticles with Heavy Metal Ions: A New Strategy for Probe Design. *Anal. Chem.* **2016**, *88*, 9989−9995.

(24) Peng, J.; Xu, W.; Teoh, C. L.; Han, S.; Kim, B.; Samanta, A.; Er, J. C.; Wang, L.; Yuan, L.; Liu, X.; Chang, Y. T. High-efficiency in vitro and in vivo detection of Zn2+ by dye-assembled upconversion nanoparticles. *J. Am. Chem. Soc.* **2015**, *137*, 2336−2342.

(25) Nagai, A.; Miller, J. B.; Kos, P.; Elkassih, S.; Xiong, H.; Siegwart, D. J. Tumor Imaging Based on Photon Upconversion of Pt(II) Porphyrin Rhodamine Co-modified NIR Excitable Cellulose Enhanced by Aggregation. *ACS Biomater. Sci. Eng.* **2015**, *1*, 1206−1210.
(26) Zhu, X.; Su, Q.; Feng, W.; Li, F. Anti-Stokes shift luminescent materials for bio-applications. *Chem. Soc. Rev.* **2017**, *46*, 1025−1039.
(27) Zhou, J.; Liu, Q.; Feng, W.; Sun, Y.; Li, F. Upconversion Luminescent Materials: Advances and Applications. *Chem. Rev* **2015**, *115*, 395−465.
(28) Xie, L.; Qin, Y.; Chen, H.-Y. Polymeric Optodes Based on Upconverting Nanorods for Fluorescent Measurements of pH and Metal Ions in Blood Samples. *Anal. Chem.* **2012**, *84*, 1969−1974.
(29) Wu, J.; Qin, Y. Polymeric optodes based on upconverting nanorods for fluorescence measurements of Pb^{2+} in complex samples. *Sens. Actuators, B* **2014**, *192*, 51−55.
(30) Chen, G.; Qiu, H.; Prasad, P. N.; Chen, X. Upconversion Nanoparticles: Design, Nanochemistry, and Applications in Theranostics. *Chem. Rev.* **2014**, *114*, 5161−5214.
(31) Ge, X.; Sun, L.; Ma, B.; Jin, D.; Dong, L.; Shi, L.; Li, N.; Chen, H.; Huang, W. Simultaneous realization of Hg^{2+} sensing, magnetic resonance imaging and upconversion luminescence in vitro and in vivo bioimaging based on hollow mesoporous silica coated UCNPs and ruthenium complex. *Nanoscale* **2015**, *7*, 13877−13887.
(32) Xie, L.; Qin, Y.; Chen, H.-Y. Direct Fluorescent Measurement of Blood Potassium with Polymeric Optical Sensors Based on Upconverting Nanomaterials. *Anal. Chem.* **2013**, *85*, 2617−2622.
(33) Galyean, A. A.; Behr, M. R.; Cash, K. J. Ionophore-based optical nanosensors incorporating hydrophobic carbon dots and a pH-sensitive quencher dye for sodium detection. *Analyst* **2018**, *143*, 458−465.
(34) Ferris, M. S.; Katageri, A. G.; Gohring, G. M.; Cash, K. J. A dual-indicator strategy for controlling the response of ionophore-based optical nanosensors. *Sens. Actuators, B* **2018**, *256*, 674−681.
(35) Simon, Y. C.; Weder, C. Low-power photon upconversion through triplet-triplet annihilation in polymers. *J. Mater. Chem.* **2012**, *22*, 20817−20830.
(36) Liu, Q.; Yin, B.; Yang, T.; Yang, Y.; Shen, Z.; Yao, P.; Li, F. A general strategy for biocompatible, high-effective upconversion nanocapsules based on triplet-triplet annihilation. *J. Am. Chem. Soc.* **2013**, *135*, 5029−5037.
(37) Wohnhaas, C.; Friedemann, K.; Busko, D.; Landfester, K.; Baluschev, S.; Crespy, D.; Turshatov, A. All Organic Nanofibers As Ultralight Versatile Support for Triplet-Triplet Annihilation Upconversion. *ACS Macro Lett.* **2013**, *2*, 446−450.
(38) Liu, Q.; Yang, T.; Feng, W.; Li, F. Blue-emissive upconversion nanoparticles for low-power-excited bioimaging in vivo. *J. Am. Chem. Soc.* **2012**, *134*, 5390−5397.
(39) Kwon, O. S.; Song, H. S.; Conde, J.; Kim, H. I.; Artzi, N.; Kim, J. H. Dual-color emissive upconversion nanocapsules for differential cancer bioimaging in vivo. *ACS Nano* **2016**, *10*, 1512−1521.
(40) Liu, Y.; Su, Q.; Zou, X.; Chen, M.; Feng, W.; Shi, Y.; Li, F. Near-infrared: In vivo bioimaging using a molecular upconversion probe. *Chem. Commun.* **2016**, *52*, 7466−7469.
(41) Tian, B.; Wang, Q.; Su, Q.; Feng, W.; Li, F. In-vivo biodistribution and toxicity assessment of triplet-triplet annihilation-based upconversion nanocapsules. *Biomaterials* **2017**, *112*, 10−19.
(42) Askes, S. H. C.; Leeuwenburgh, V. C.; Pomp, W.; Arjmandi-Tash, H.; Tanase, S.; Schmidt, T.; Bonnet, S. Water-dispersible silica-coated upconverting liposomes: can a thin silica layer protect TTA-UC against oxygen quenching? *ACS Biomater. Sci. Eng.* **2017**, 322−334.
(43) Wohnhaas, C.; Mailänder, V.; Dröge, M.; Filatov, M. A.; Busko, D.; Avlasevich, Y.; Baluschev, S.; Miteva, T.; Landfester, K.; Turshatov, A. Triplet-triplet annihilation upconversion based nanocapsules for bioimaging under excitation by red and deep-red light. *Macromol. Biosci.* **2013**, *13*, 1422−1430.
(44) Wohnhaas, C.; Turshatov, A.; Mailänder, V.; Lorenz, S.; Baluschev, S.; Miteva, T.; Landfester, K. Annihilation Upconversion in Cells by Embedding the Dye System in Polymeric Nanocapsules. *Macromol. Biosci.* **2011**, *11*, 772−778.
(45) Borisov, S. M.; Larndorfer, C.; Klimant, I. Triplet-triplet annihilation-based anti-stokes oxygen sensing materials with a very broad dynamic range. *Adv. Funct. Mater.* **2012**, *22*, 4360−4368.
(46) Sahari, A.; Ruckh, T. T.; Hutchings, R.; Clark, H. A. Development of an Optical Nanosensor Incorporating a pH-Sensitive Quencher Dye for Potassium Imaging. *Anal. Chem.* **2015**, *87*, 10684−10687.
(47) Ferris, M. S.; Behr, M. R.; Cash, K. J. An ionophore-based persistent luminescent 'Glow Sensor' for sodium detection. *RSC Adv.* **2019**, *9*, 32821−32825.
(48) Billingsley, K.; Balaconis, M. K.; Dubach, J. M.; Zhang, N.; Lim, E.; Francis, K. P.; Clark, H. A. Fluorescent Nano-Optodes for Glucose Detection. *Anal. Chem.* **2010**, *82*, 3707−3713.
(49) Cash, K. J.; Clark, H. A. Phosphorescent Nanosensors for *In Vivo* Tracking of Histamine Levels. *Anal. Chem.* **2013**, *85*, 6312−6318.
(50) Dubach, J. M.; Balaconis, M. K.; Clark, H. A. Fluorescent Nanoparticles for the Measurement of Ion Concentration in Biological Systems. *J. Visualized Exp.* **2011**, 1−5.
(51) Kirchner, S.; Fothergill, J. L.; Wright, E. A.; James, C. E.; Mowat, E.; Winstanley, C. Use of Artificial Sputum Medium to Test Antibiotic Efficacy Against Pseudomonas aeruginosa in Conditions More Relevant to the Cystic Fibrosis Lung. *J. Visualized Exp* **2012**, *64*, 7.
(52) Jewell, M. P.; Galyean, A. A.; Kirk Harris, J.; Zemanick, E. T.; Cash, K. J. Luminescent Nanosensors for Ratiometric Monitoring of Three-Dimensional Oxygen Gradients in Laboratory and Clinical *Pseudomonas aeruginosa* Biofilms. *Appl. Environ. Microbiol.* **2019**, *85*, e01116−e01119.
(53) Islangulov, R. R.; Lott, J.; Weder, C.; Castellano, F. N. Noncoherent low-power upconversion in solid polymer films. *J. Am. Chem. Soc.* **2007**, *129*, 12652−12653.
(54) Monguzzi, A.; Tubino, R.; Meinardi, F. Upconversion-induced delayed fluorescence in multicomponent organic systems: Role of Dexter energy transfer. *Phys. Rev. B* **2008**, *77*, 155122.
(55) Monguzzi, A.; Frigoli, M.; Larpent, C.; Tubino, R.; Meinardi, F. Low-power-photon up-conversion in dual-dye-loaded polymer nanoparticles. *Adv. Funct. Mater.* **2012**, *22*, 139−143.
(56) Keivanidis, P. E.; Baluschev, S.; Miteva, T.; Nelles, G.; Scherf, U.; Yasuda, A.; Wegner, G. Up-Conversion Photoluminescence in Polyfluorene Doped with Metal(II)−Octaethyl Porphyrins. *Adv. Mater.* **2003**, *15*, 2095−2098.
(57) Shortreed, M. R.; Dourado, S.; Kopelman, R. Development of a fluorescent optical potassium-selective ion sensor with ratiometric response for intracellular applications. *Sens. Actuators, B* **1997**, *38*, 8−12.
(58) Zhai, J.; Xie, X.; Bakker, E. Solvatochromic Dyes as pH-Independent Indicators for Ionophore Nanosphere-Based Complexometric Titrations. *Anal. Chem.* **2015**, *87*, 12318−12323.
(59) Xie, X.; Szilagyi, I.; Zhai, J.; Wang, L.; Bakker, E. Ion-Selective Optical Nanosensors Based on Solvatochromic Dyes of Different Lipophilicity: From Bulk Partitioning to Interfacial Accumulation. *ACS Sens.* **2016**, *1*, 516−520.
(60) Marsico, F.; Turshatov, A.; Peköz, R.; Avlasevich, Y.; Wagner, M.; Weber, K.; Donadio, D.; Landfester, K.; Baluschev, S.; Wurm, F. R. Hyperbranched Unsaturated Polyphosphates as a Protective Matrix for Long-Term Photon Upconversion in Air. *J. Am. Chem. Soc.* **2014**, *136*, 11057−11064.
(61) Mistlberger, G.; Crespo, G. A.; Bakker, E. Ionophore-Based Optical Sensors. *Annu. Rev. Anal. Chem.* **2014**, *7*, 483−512.